

# Investigation of Electroacoustic Properties of Experimental Fibre-Optic Microphone Designs

Florian Klein<sup>1</sup>, Christoph Ferdinand Hemeling<sup>2</sup>, Andreas Männchen<sup>1</sup>,  
Marvin Henkel<sup>2</sup>, Daniel Beer<sup>1</sup>, Thomas Kissinger<sup>2</sup>, Joachim Bös<sup>1</sup>

<sup>1</sup> Fraunhofer Institute for Digital Media Technology IDMT, 98693 Ilmenau, Germany

<sup>2</sup> Nanofabrication and Nanomeasurement Technology Group, Technische Universität Ilmenau, 98693 Ilmenau, Germany

Email: [florian.klein@idmt.fraunhofer.de](mailto:florian.klein@idmt.fraunhofer.de)

## Introduction

Investigating Fiber Optic Strain Sensing in acoustics offers possible advantages for specialized use cases, such as insensitivity to electromagnetic interference (EMI), suitability for high-temperature environments and the possibility to integrate fibers into structural elements. Currently, fiber-optic sensing is considered for hydrophones or by using existing underwater cables to monitor whales. Another well known use case is the monitoring of pipelines to identify leaks, of structural health issues or of third party interferences. However, applications for airborne sound microphones have only been studied rarely until now. In this study, we present three different implementations of a fiber-optic microphone (FOM) based on fiber-optic strain measurements utilizing fiber segment interferometry (FSI) built upon range-resolved interferometry (RRI). We compare these designs in terms of sensitivity, signal-to-noise ratio and the resonance behavior of the system. Our aim is to estimate the potentials and drawbacks of the working principle in order to identify use cases where it excels.

## Basics of FSI and Related Work

Strain measurements in optical fibers can be accomplished using various methods, with fiber Bragg grating (FBG) strain sensors being a well-established commercial technology. However, they are limited in the gauge length to  $\approx$  cm and can be sensitive to strain gradients. Conversely, the Fiber Segment Interferometry (FSI) approach used in this paper allows to use sensing segments of fully customizable gauge length ( $\approx$  cm to m). FSI is based on the RRI signal processing scheme, which utilizes the sinusoidal modulation of a laser diode's optical frequency to demodulate interferometric signals according to their optical path differences, achieving high linearity [1]. FSI demonstrates superior strain resolution compared to FBG sensors, as evidenced by comparative studies conducted by Barrington et al. [2]. Additionally, FSI has shown reliability in challenging measurement environments, such as on helicopter rotor blades at full speed [3]. In contrast to FBG-based interrogation, FSI can be implemented with cost-effective laser diodes originating from the telecoms industry. For practical implementation, signal processing libraries and hardware recommendations are available through the OpenRRI Project [4].

The basic principle of FSI is shown in Figs. 1. The sinusoidal modulation of the input laser wavelength im-

poses range-dependent carrier functions on the photodetector signal. By selecting the desired range channels, signals from multiple interferometric reflectors within the fibre can be evaluated simultaneously and strain-induced changes in their optical path lengths in the corresponding segments interrogated with sub-nanometer resolution. Furthermore, through the use of multiple parallel fibers, fiber optic shape sensing can also be implemented with FSI [5]. This allows for the investigation of structural dynamics with high resolution [6], potentially permitting the identification of transducer mode shapes in the audio-frequency domain in future investigations.

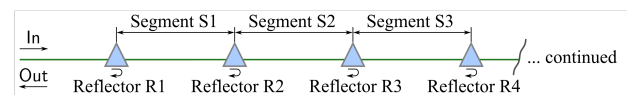


**Figure 1:** Basic FSI Concept: Partial reflectors are embedded in the fiber-optical cable and are used to divide the cable into sensing segments.

## Experimental FOM Designs and Measurement Setup

Fig. 2 shows a schematic of the setup used to investigate the three different FOM designs. Here, the input sinusoidal wavelength modulation needed for the RRI signal processing scheme, is realized by the modulation of injection current of a 1550 nm laser diode. Light is then coupled into different measurement channels, where interferometric segments are formed by the Fresnel reflections occurring at a flat-polished ferrule tip and the cleaved fiber end face, respectively. The return signal caused by these reflections is then recorded by photo detectors. In a post-processing step, the interferometric phase signal is then demodulated using the OpenRRI Python library.

With the goal of compensating for temperature-induced drifts and reducing noise due to laser line width through differential measurement, a reference fiber of similar length as the sensing fibers was placed near the sensor for each measurement. However, in later analysis, it was evident that reference fibers were also affected by the audio signal, and therefore, the difference signal between reference and sensing fiber did not yield the expected reduction in noise floor.

Overall, three different FOM designs have been built and measured in an anechoic chamber. The microphones

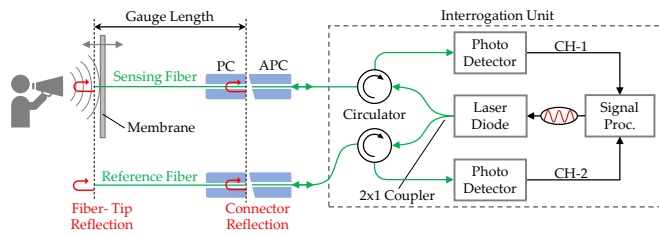


**Figure 2:** Schematic of the experimental setup. The strain in the segment between the diaphragm and the interconnectors (labeled PC and APC) is measured.

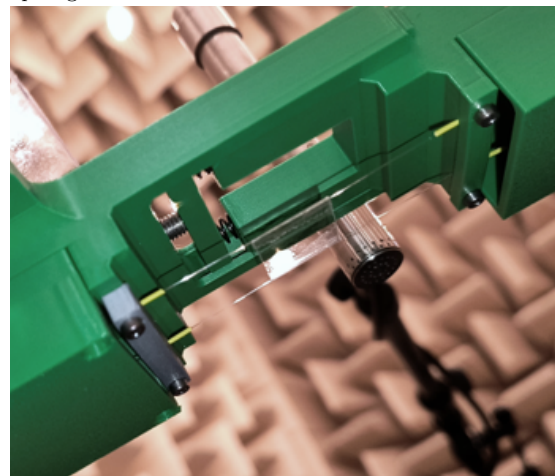
were placed 80 cm above a Genelec 8341A coaxial speaker, which was directed upwards. A Microtech Gefell MK 221 measurement microphone was placed close to each FOM diaphragm and the output level of the speaker was adjusted to yield 90 dB sound pressure level (SPL) at the measurement distance (min.: 84 dB, max.: 93 dB), keeping the loudspeaker in a linear operating range. Fig. 3 shows all three FOM designs. In the case of the hanging plate (Fig. 3a), the diaphragm is suspended on three sensing fibers. Using additional weights, different diaphragm masses are realized in a range from approx. 9 g to 37 g. This way, the optical fibers act as a pre-tensioned spring and a change in pressure results in a change of strain. Our aim was to search for an optimal mass in order to maximize sensitivity. The second FOM design is realized in form of two fibers pre-tensioned like guitar strings (Fig. 3b). A small patch of sticky tape attached to the fibers acts as a diaphragm. The third microphone design was implemented as a tensegrity structure (Fig. 3c). The diaphragm (shown in blue) is suspended under opposing tension between the optical fibers (shown in yellow) and an inelastic tension cable (shown in orange), which is attached to the diaphragm by an extension spring. The red arrows visualize the tension of the elements. The preload on the optical fibers is introduced by the centric spring, which benefits the load distribution. By winding the tension cable, the preload can be adjusted continuously. The strings in the tensegrity design have the advantage, that the mass of the diaphragm is decoupled from the applied tension to the sensing fibers as in comparison to the hanging plate design. However this resulted in a practical problem: The tension force applied to the fibers can be estimated by the coiled fiber length, but only with a low accuracy due to manual adjustment. Different tensions were set, in 5 steps in case of the string design and in 7 steps in case of the tensegrity design).

### Measurement Evaluation

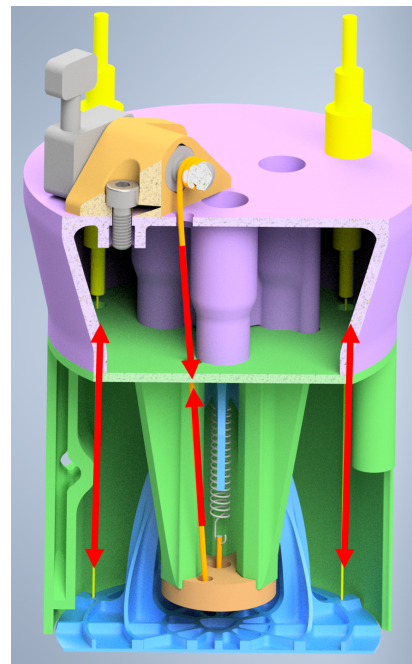
Using the data from the aforementioned measurement setup, the three different FOM designs and their various configurations (different weights, different tensions) can be compared in terms of typical microphone parameters. In this study, we focus mainly on the sensitivity  $S(f)$  at each frequency, i.e., the microphone output as a (calculated) response to a sinusoidal stimulus at 94 dB SPL, the root-mean-square (RMS) noise floor (measured with a turned-off loudspeaker) in a bandwidth from 20 Hz to 20 kHz, denoted as  $N_{FBW}$ , as well as in third-octave



(a) The 'hanging plate' design with an effective diaphragm area of 82.3 cm<sup>2</sup>.



(b) The 'strings' design with an effective diaphragm area of 3 cm<sup>2</sup>.



(c) The 'tensegrity' design with an effective diaphragm area of 36.3 cm<sup>2</sup>.

**Figure 3:** Depictions of the three investigated FOM designs.

bands, and the signal-to-noise ratio (SNR). The latter is also computed at each frequency as

$$\text{SNR}(f) = S(f) - N_{\text{FBW}}, \quad [\text{dB}] \quad (1)$$

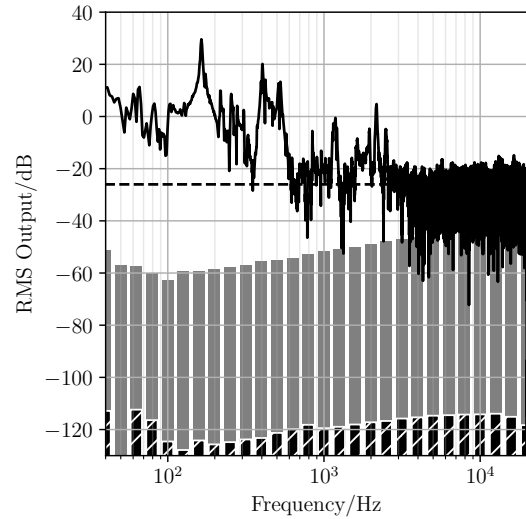
with all quantities being in dB, having a reference value of 1, and applying no frequency-weighting. For each FOM design, Fig. 4 displays the sensitivity and third-octave noise floor of the best-performing configuration with respect to mean SNR. The highest SNR for the ‘hanging plate’ design was achieved with a diaphragm mass of approx. 27 g. The ‘strings’ design was not significantly affected by changing the tension, probably due to a sub-optimal build, reaching its highest SNR at tension setting 1 out of 5. Finally, the ‘tensegrity’ design showed only slight changes in sensitivity as a function of tension and performed best using tension setting 6 out of 7.

Tab. 1 gives an overview of the measurement results for each best-performing configuration. In addition to presenting just the measured values (meas.) of the sensitivity and the SNR, it also gives values for each quantity that compensate (comp.) for the different diaphragm areas so as to represent the theoretical performance that would be achieved with a ½” diaphragm (like the reference microphone).

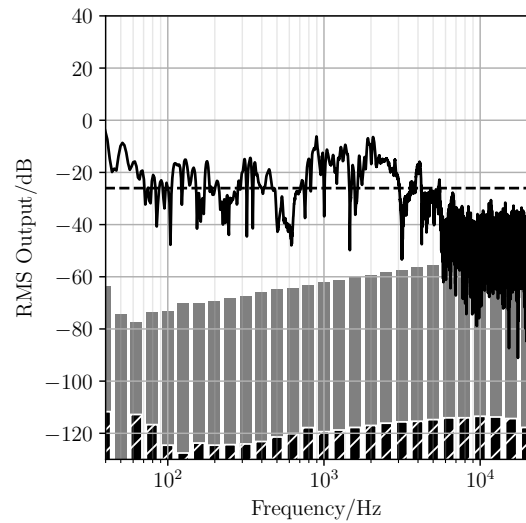
A common metric to compare FOM is the minimum detectable sound pressure level (MDSPL) at 1 kHz. Tab. 2 shows the MDSPL and the noise around 1 kHz for each of the three FOM designs, as calculated according to the descriptions given in [7].

### Discussion and Comparison

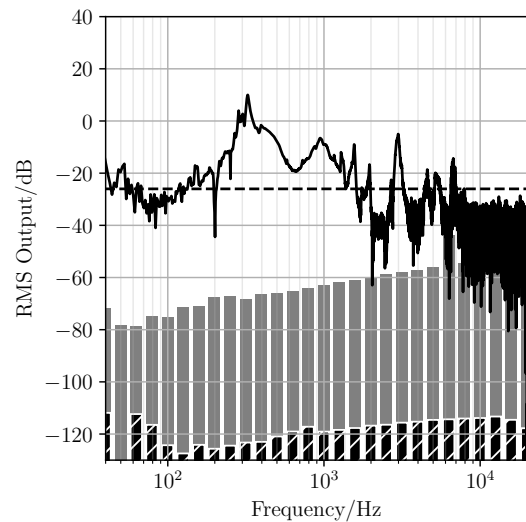
All microphone designs exhibit strongly resonant behavior, particularly within the hearing range. Considering the FOM as spring-mass systems, there are generally two basic options to shift the resonances higher: either by using a lighter diaphragm (mass) or by increasing fiber (spring) tension. While it was possible to find an optimal mass for the ‘hanging plate’ design, there was no obvious optimum tension setting in the case of the other two designs. Likely, this is related to the employed mechanics, which did not allow us to set a defined force. Additionally, the low SNR presents a challenge: With mean SNR values from 26 dB to 32 dB these experimental designs are clearly inferior to the reference microphone (mean SNR: 75 dB). The source of the noise remains currently unclear, but based on the reference microphone performance being as good as expected, it does not seem to originate from acoustic sources, suggesting the issue may lie in the mechanical-to-optical or optical-to-electrical conversion stages. This is supported by the different noise levels found in each design, with the ‘hanging plate’ design deviating strongly. In addition, the reference fiber was not placed optimally, therefore not being suitable for the differential measurement that was supposed to significantly reduce the potential noise. In spite of the noise levels, the MDSPL values generally lie in the range of other FOM designs previously reported in the literature. However, some state-of-the-art FOM designs have reached MDSPL values below -20 dB (1.9 μPa/√Hz noise) [7].



(a) The ‘hanging plate’ design.



(b) The ‘strings’ design.



(c) The ‘tensegrity’ design.

**Figure 4:** Depiction of sensitivity and noise floor of the three FOM designs, displaying the measurements with the highest mean SNR. Sensitivity of FOM (solid line) and reference microphone (dashed line) as well as third-octave noise floor of FOM (gray bars) and reference microphone (hatched white-on-black bars) are shown.

**Table 1:** Measurement results for the configuration with the highest mean SNR of each design. Mean and maximum sensitivity and SNR are given as measured (meas.) values and theoretical values that are compensated (comp.) to represent the performance that would be achieved with a 1/2" diaphragm.

Design	Config.	Sensitivity/dB				N <sub>FBW</sub> /dB	SNR/dB			
		meas.		comp.			meas.		comp.	
		mean	max	mean	max		mean	max	mean	max
hanging plate	weight 27 g	-1.0	29.0	-37.3	-7.2	-32.8	31.8	61.8	-4.5	25.6
string	tension 1 of 5	-21.4	-4.3	-30.2	-13.1	-43.3	21.9	39.0	13.1	30.2
tensegrity	tension 5 of 7	-15.0	10.0	-44.2	-19.2	-41.1	26.0	51.0	-3.1	21.9

**Table 2:** Comparison of the MDSPL of the three FOM designs. Values taken from the configuration with the highest mean SNR of each design.

Design	Config.	MDSPL @ 1 kHz/dB	Noise around 1 kHz/(μPa/√Hz)
hanging plate	weight 27 g	35.1	1100
string	tension 1 of 5	31.8	778
tensegrity	tension 5 of 7	16.7	137

### Conclusion

The results clearly show that this FOM approach has potential but, at the same time, they reveal some problems that will need to be resolved to tap into that potential. Identifying the noise source and examining the spring-like behavior of the fibers are the most important steps at the current development stage. To increase the sensitivity of the FOM, the optical path difference needs to be increased for a given SPL. As shown by Zhang et al. [7] this could be done by wrapping a fiber around a cylinder. In general, the optical fibers need to be attached to a deformable object or to a diaphragm in a classical sense to induce strain to the fibers. Compared to condenser microphones, the diaphragm can be made of a wide range of materials. The material selection can be guided by the use case and could feature, e.g., high temperature resistance, EMI insensitivity, or bio-compatibility. The diaphragm may also be part of a structural element and, thus, be integrated directly into the housing of a machine.

Finally, the benefits of FSI have not been utilized yet: Our experiments only used a single segment. Multiple segments could be used to increase the sensitivity through averaging or by tuning the acoustic-to-mechanical conversion optimum in each segment to a certain frequency.

Overall, a lot of potential for improvements has been identified, and future development should be driven by an application that builds upon the strengths of the general approach.

### References

[1] T. Kissinger, T. O. Charrett, and R. P. Tatam, "Range-resolved interferometric signal processing using sinusoidal optical frequency modulation," *Opt. Express*, vol. 23, no. 7, pp. 9415–9431, 2015. [Online]. Available: <https://opg.optica.org/oe/abstract.cfm?URI=oe-23-7-9415>

[2] J. H. Barrington, T. Kissinger, S. W. James, and R. P. Tatam, "Direct comparison of the strain measurement performance of fibre bragg gratings and fibre segment interferometry," 2023, p. W4.83. [Online]. Available: <https://opg.optica.org/abstract.cfm?URI=OFS-2023-W4.83>

[3] S. W. James, T. Kissinger, S. Weber, K. Mullaney, E. Chehura, H. H. Pekmezci, J. H. Barrington, S. E. Staines, T. O. H. Charrett, N. J. Lawson, M. Lone, R. Atack, and R. P. Tatam, "Fibre-optic measurement of strain and shape on a helicopter rotor blade during a ground run: 1. measurement of strain," *SMS*, vol. 31, no. 7, p. 075014, 2022. [Online]. Available: <https://dx.doi.org/10.1088/1361-665X/ac736d>

[4] G. Straube, C. Hemeling, F. Schwesinger, V. Shmagun, A. Barth, J. S. F. Calderón, and T. Kissinger, "OpenRRI: theory and application of open-source interferometry," vol. 12997:1L, 2024.

[5] T. Kissinger, E. Chehura, S. E. Staines, S. W. James, and R. P. Tatam, "Dynamic fiber-optic shape sensing using fiber segment interferometry," *J. Lightwave Technol.*, vol. 36, no. 4, pp. 917–925, 2018. [Online]. Available: <https://opg.optica.org/jlt/abstract.cfm?URI=jlt-36-4-917>

[6] S. Weber, T. Kissinger, E. Chehura, S. Staines, J. Barrington, K. Mullaney, L. Z. Fragonara, I. Petrunin, S. James, M. Lone, and R. Tatam, "Application of fibre optic sensing systems to measure rotor blade structural dynamics," *Mechanical Systems and Signal Processing*, vol. 158, p. 107758, 2021. [Online]. Available: <https://www.sciencedirect.com/science/article/pii/S0888327021001539>

[7] B. Zhang, K. Chen, M. Guo, C. Li, C. Li, Y. Yang, W. Peng, and Q. Yu, "Dual enhanced fiber-optic microphone using sensitive diaphragm-free transducer and ultrahigh-resolution spectral demodulation," *IEEE Transactions on Instrumentation and Measurement*, vol. 70, pp. 1–8, 2021.